Determination of the Dynamics of Healing at the Tissue-Implant Interface by Means of Microcomputed Tomography and Functional Apparent Moduli

Po-Chun Chang, DDS, PhD[1], **Yang-Jo Seol, DDS, PhD**[2], **Steven A. Goldstein, PhD**[3], and **William V. Giannobile, DDS, DMSc**[4]

[1]Researcher, Department of Periodontics and Oral Medicine, School of Dentistry; Researcher, Department of Biomedical Engineering, College of Engineering, University of Michigan, Ann Arbor, Michigan, USA; Current Position, Assistant Professor, Discipline of Periodontics, Faculty of Dentistry, National University of Singapore, Singapore

[2]Researcher, Department of Periodontics and Oral Medicine, School of Dentistry, University of Michigan, Ann Arbor, Michigan, USA; Current Position, Associate Professor, Department of Periodontology, School of Dentistry, Seoul National University, Seoul, Korea

[3]Professor, Department of Biomedical Engineering, College of Engineering; Professor, Department of Orthopedic Surgery, School of Medicine, University of Michigan, Ann Arbor, Michigan, USA

[4]Professor, Department of Periodontics and Oral Medicine, School of Dentistry; Professor, Department of Biomedical Engineering, College of Engineering; Director, Michigan Center for Oral Health Research, School of Dentistry, University of Michigan, Ann Arbor, Michigan, USA

Abstract

Purpose—It is currently a challenge to determine the biomechanical properties of the hard tissue–dental implant interface. Recent advances in intraoral imaging and tomographic methods, such as microcomputed tomography (micro-CT), provide three-dimensional details, offering significant potential to evaluate the bone-implant interface, but yield limited information regarding osseointegration because of physical scattering effects emanating from metallic implant surfaces. In the present study, it was hypothesized that functional apparent moduli (FAM), generated from functional incorporation of the peri-implant structure, would eliminate the radiographic artifact– affected layer and serve as a feasible means to evaluate the biomechanical dynamics of tissue-implant integration in vivo.

Materials and Methods—Cylindric titanium mini-implants were placed in osteotomies and osteotomies with defects in rodent maxillae. The layers affected by radiographic artifacts were identified, and the pattern of tissue-implant integration was evaluated from histology and micro-CT images over a 21-day observation period. Analyses of structural information, FAM, and the

relationship between FAM and interfacial stiffness (IS) were done before and after eliminating artifacts.

Results—Physical artifacts were present within a zone of about 100 to 150 μm around the implant in both experimental defect situations (osteotomy alone and osteotomy + defect). All correlations were evaluated before and after eliminating the artifact-affected layers, most notably during the maturation period of osseointegration. A strong correlation existed between functional bone apparent modulus and IS within 300 μm at the osteotomy defects (r > 0.9) and functional composite tissue apparent modulus in the osteotomy defects (r > 0.75).

Conclusion—Micro-CT imaging and FAM were of value in measuring the temporal process of tissue-implant integration in vivo. This approach will be useful to complement imaging technologies for longitudinal monitoring of osseointegration.

Keywords

biomechanics; dental implants; finite element analysis; microcomputed tomography

The establishment of firm anchorage within the alveolar bone is crucial to ensure the clinical success of dental implant treatment. Implant stability is affected by several factors, including the stiffness of the implants, implant design, surgical procedures, bone-implant contact relationship, and the quality of the implant-supporting bone.[1–3] Excessive mobility of implants may lead to fibrous tissue encapsulation and aggressive destruction of peri-implant tissue.[4] Osseointegration, the formation of a direct bone-to-implant interface without intervening tissue,[5] is one of the prerequisites to achieve implant stability. The dynamics of osseointegration are determined by bone apposition in the early stages and remodeling in later stages.[6] Current preclinical investigations of osseointegration have relied mostly on structural analyses from histology or radiography. However, these two-dimensional images provide limited information,[7] and poor correlation between histology and radiography near the implant surface has also been noted.[8] A clinical study also demonstrated a discrepancy between histology and cone beam computed tomography, although the trend of osteogenesis appeared similar.[9] As such, Park and colleagues demonstrated that three-dimensional microcomputed tomography (micro-CT) was capable of accurately identifying mineralized tissues within the dentoalveolar complex.[10] However, the unavoidable metal scatter surrounding the titanium implant severely limits the usefulness of micro-CT to investigate bone-implant interfaces in vivo.[11]

Since the introduction of several biomechanical test methods for preclinical and clinical implant stability measurements,[12,13] some studies have demonstrated correlations between biomechanical tests and histomorphometric parameters, including bone-implant contact[14] or bone area adjacent to the implant.[15] However, those studies did not focus on the differences between histologic and biomechanical testing methods. Parameters from three-dimensional images prior to or after implant removal may overcome this limitation, but the correlations between interfacial biomechanics and individual parameters remain unclear.[16–19] This might be a result of the lack of comprehensive consideration of the effects from structures and the limitations of study design. Thus, the present authors developed functional apparent moduli (FAM) to serve as the effective stiffness of the peri-implant tissue by incorporation of three-

dimensional structures from micro-CT and applied a simulated oral functional load on the oral implants.[20] FAM was calculated through the numeric converging of finite element (FE) optimization processes, and it was previously demonstrated that FAM was more strongly correlated to interfacial stiffness (IS) and implant removal torque than any structural parameter. FAM was also correlated to the growth patterns and represented the biomechanical function of peri-implant tissue during tissue-implant integration. The study demonstrated that the most biomechanically relevant peri-implant layer was about 200 μm from the implant with intact alveolar bone support and 575 μm in an area with a preexisting osseous defect.

With tissue-implant integration accepted as a progressive and dynamic process of bone apposition and remodeling, it is hypothesized that the peri-implant structure should reveal a clinical value for determining the tissue-implant interfacial biomechanics while accurately compensating for radiographic artifacts. An in vivo implant osseointegration model was utilized in which the physical artifacts between the tissue-implant interface were identified from micro-CT imaging. The correlation of peri-implant structure, FAM, and functional relevance of peri-implant structure integration was determined in the context of determining the functional support from peri-implant tissue in vivo.

MATERIALS AND METHODS

Animals and Study Materials

Fifty male Sprague-Dawley rats were utilized in this study (2 for radiographic determination, 36 for evaluation of functional dynamics during tissue-implant integration, and 12 for histologic observations). All related procedures followed the guidelines of the University Committee on the Use and Care of Animals at the University of Michigan, and the sample size was six per group per time point, based on the information from relevant studies.[7,21] The cylindric titanium implants utilized in this study were 1 mm in diameter and 2 mm in length and featured the SLActive surface (Institut Straumann).

Implant Osseointegration Model

Prior to tooth extraction and implant placement, animals were anesthetized with a combination of ketamine (50 mg/kg) and xylazine (10 mg/kg); analgesia was then induced with buprenorphine (0.1 to 0.5 mg/kg). Antibiotic water (268 mg ampicillin in 1 L 5% dextrose water) was provided for 7 to 10 days postsurgery. Bilaterally, the maxillary molars were extracted from all experimental animals. After a healing period of 28 to 30 days, a 0.95-mm-diameter osteotomy was made on the edentulous ridge of the maxilla in all animals (OA group, Fig 1a); a 0.6×1-mm coronal osseous defect surrounding the osteotomy was created in a randomly selected side in half of the animals (OS group, Fig 1b). Implants were then press-fit into the osteotomy sites, with the top of each implant kept level with the alveolar crest. Type 1 collagen matrix (Tissue Repair Company) containing a gene vector reporter (adenoviral- encoding luciferase)[22] was delivered to the osseous defect area. The implant sites were closed with butyl cyanoacrylate (PeriAcryl, GluStitch). Animals were sacrificed after 10, 14, and 21 days. Two maxillae per group per time point were dissected

for histologic observation, and the remaining six maxillae were used for micro-CT imaging and biomechanical testing.

Radiographic Determinations

In two fresh cadaver specimens, 0.6×1-mm circumferential osseous defects with 0.95-mm-diameter penetrating osteotomies were created in the harvested maxillae. Micro-CT scanning was performed using a GFHS Micro-CT system under high voltage (90 kV) with a copper filter to eliminate the beam-hardening effect (Fig 2). The images were reconstructed with a voxel size of $18 \times 18 \times 18$ μm^3. After the first scan, the titanium implants were press-fitted into the osteotomy site, and a micro-CT scan was performed subsequently using the same settings. Commercialized CT phantoms (Gammex) with electronic density values of 1.09, 1.47, and 1.69 (density values of 723 ± 51 Hounsfield units [HU], $1,064 \pm 82$ HU, and $1,201 \pm 58$ HU, respectively) were used in each scan to calibrate all the micro-CT images, and the images were filtered and analyzed by Micro-View Analysis software (GE Healthcare). Mesiodistal straight lines traversing the middle region of each osseous defect (yellow lines in Fig 2b and 2c) and osteotomy (blue line in Figs 2b and 2c) were drawn on the central sagittal plane of the osteotomy site (grey plane in Fig 2a), and the HU values of voxels on this trajectory were recorded.

Histologic Observation

The specimens were fixed in 50% ethanol for at least 72 hours and then embedded in epoxy resin. The block biopsy specimens were then sectioned by a diamond saw blade (Crystalite) in the longitudinal direction and polished to achieve a final thickness of 50 to 100 μm. The sections were then stained with methylene blue and counterstained with acid fuchsin.

Implant Biomechanical Testing and Micro-CT Imaging

Initial micro-CT images were captured prior to implant removal under the previously described conditions. The images were reoriented, and the position of each implant was identified using a customized computer algorithm. The maxillae were then secured in acrylic resin and mounted on a metal stage. Biomechanical testing was performed with an MTS machine (Model 858, Mini-Bionix II, MTS Systems) by pushing the implant out at a constant displacement rate of 0.1 mm/s. The load-displacement relationship was recorded during the procedure. The IS was calculated using the slope of a tangent at the load-displacement curve. Micro-CT images were obtained again after the implants had been removed; then the images were reoriented and the position of each implant was identified using an automated computer algorithm.

The correlation between the micro-CT parameters in the cumulative concentric peri-implant layer and interfacial biomechanics was investigated on the basis of an 18-μm thickness. Based on the results from the radiographic determination in the present study, the innermost peri-implant layer significantly affected by metal scattering was eliminated from the image to evaluate the influence of metal scattering on the correlations.

Functional Apparent Moduli

The micro-CT images were segmented and homogenized to establish FE models as previously described.[20] Two axisymmetric FE models were established (Figs 3a to 3d) from the same micro-CT image, and both received an identical simulated load from the dental implant for each integrated parameter. In the microscopic model, the spatial information and local elasticity of the entire peri-implant structure were projected and calculated from the micro-CT based on an algorithm provided by Keller[23]; in the optimizing model, the concentric peri-implant tissue of interest was assumed to be homogenous and the functional elasticity was determined from the numeric optimization process of the microscopic model. The Young's modulus was set at 200 MPa for the granulation tissue[24] and 110 GPa for the implant. The Poisson ratio for all the peri-implant elements was set at 0.3, except for the granulation tissue, which was set at 0.167, and the implant, which was set at 0.35.[24,25] The FE simulation was processed using linear static analysis (ABAQUS software, version 6.7-1, Dassault Systèmes), and optimization between the two models was processed by a customized MATLAB algorithm. The functional bone apparent modulus (FBAM), which represents the functional support of peri-implant bone against the implant loading, and the functional composite tissue apparent modulus (FCAM), which represents the functional support of the peri-implant composite tissue against implant loading, were evaluated in the osseous defect area (Figs 3a and 3d) and peri-implant concentric layers (Figs 3b and 3c) within the thickness of 600 μm.

Influence of Radiographic Artifacts on Assessment of Peri-Implant Tissues

To determine the correlations between parameters before and after eliminating the radiographic artifacts, the innermost peri-implant layer significantly affected by metal scattering was removed from the micro-CT imaging. Micro-CT parameters; including bone volume (BV), bone mineral content (BMC; indicates the total mineral weight), and bone mineral density (BMD; indicates the average mineral weight of bone tissue); and FAM in the osseous defect area, before and after eliminating the innermost peri-implant layer significantly affected by metal scattering within 600 μm distance from the implant interface, were analyzed by Micro-View Analysis software (GE Healthcare) and by the FE optimization process described in the present study for each specimen.

Statistical Analysis

Correlation between FAM and IS, as well as comparisons before and after eliminating the artifact layers, was determined by a Pearson correlation test; a correlation was considered strong when $r > 0.75$ and moderate when $r > 0.5$. The differences between time points and whether or not the artifact was eliminated were compared by paired t tests, and the results are presented as the means ± standard deviations of measurements, with $P < .05$ being considered statistically significant.

RESULTS

Artifacts of Micro-CT Imaging

The effects of artifacts were assessed by comparing the HU of equivalent peri-implant areas before and after implant placement. Blurred high-intensity voxels were noted in a concentric area 126 to 162 μm from the implant border in the osseous defect region and 108 μm from the implant border in the osteotomy region (Fig 2). This 108- to 162-μm region was defined as the radiographic peri-implant layer was selected (108 to 162 μm) and accounted for to evaluate the influence of metal scattering on the correlations in subsequent examinations.

Histologic Observations

Interfacial bone apposition in the OA group is shown in Figs 4a to 4f. The implant was in close contact with native bone, and a gap ranging from 0 to 50 μm (dashed line in Fig 4a) filled by new bone with poorly organized collagen fibrils was noted at day 10 (Figs 4a and 4d). By day 14, most of the new bone was replaced by well-organized and mature bone, and a significant reduction of the gap was noted (Figs 4b and 4e). By day 21, the gap was completely eliminated and occupied by less mature interfacial bone (Figs 4c and 4f).

In the OS group (Figs 4g to 4l), the primary bone spongiosa started to form from the lateral wall and bottom of the defect border at day 10 (Figs 4g and 4j). By day 14, significant progression of osteogenesis, with thicker bone trabeculae and bone apposition approaching the implant border, was evident (Figs 4h and 4k). Osseous defects were nearly completely covered by thick lamellar bone at day 21 (Figs 4i and 4l).

Elimination of Metal Scattering Artifacts During Osseous Wound Repair

The values for structural parameters and FAM increased from days 10 to 14, and a significant difference was noted for both BV and BMC ($P < .001$). Eliminating the innermost peri-implant tissue significantly decreased BV and BMC ($P < .001$) but increased FBAM and FCAM, although not significantly ($P > .05$). Although the increase in peri-implant layer removal reduced the correlation with the measurements of the entire defect area, the correlation between eliminating or not eliminating the artifact was strong in all the investigated parameters except BV and FCAM at day 10, and this correlation became stronger over time (Table 1).

Functionally Relevant Peri-Implant Layer after Artifact Elimination

Initially, the correlations between FAM and IS were investigated after implant removal (Figs 5a and 5b). Following removal of the artifact-affected layers in the OA group, FBAM revealed close correlation to IS ($r > 0.95$) from the 300-μm peri-implant layer (Fig 5a). In the OS group, although fluctuation of the correlation coefficient was seen, a strong correlation between FCAM and IS was still evident in the 300-μm radial layer ($r > 0.75$) after removing the inner 108- or 162-μm peri-implant layer (Fig 5b).

These correlations tended to be weaker with the dental implant still present, especially within the 108-μm layer in the OA group ($r < 0.2$, Fig 5c) and within the 216-μm layer in the OS group ($r < 0.5$, Fig 5d). Therefore, the correlation between FBAM and IS in the OA

group was significantly increased after removing the 108- or 162-μm layer ($r > 0.85$, Fig 5c), whereas a strong correlation existed in the OS group only after removing the 162-μm layer ($r > 0.75$, Fig 5d). These results indicated that interfacial biomechanics could be predicted with the 300-μm thickness within peri-implant tissues.

DISCUSSION

Microscopic evaluation has been regarded as the gold standard to evaluate the dynamics of osteogenesis as well as osseointegration. However, it provides only two-dimensional information, and artificial separation of tissues and implants is commonly observed.[26] Clinically, CT has been widely used in implant dentistry. CT imaging provides accurate three-dimensional information for preoperative evaluation, and the information is reliable for flapless implant placement.[27–29] Micro-CT imaging further provides precise characterization of trabecular bone structure, which is suitable for periodontal evaluation,[10] and previous studies demonstrated a close similarity of the measurements between histomorphometry and equivalent plane of micro-CT imaging.[30,31] Rebaudi and colleagues reported that micro-CT might be a good method to analyze bone apposition on the implant surface non-destructively. [32] However, because of dental implant radiographic artifacts, measurements of peri-implant structures made from micro-CT imaging and histomorphometry are poorly correlated to osseointegration in vivo.[33] The present results indicate a 108- to 162-μm zone surrounding the implant surface (Fig 2), which is comparable to a previous investigation,[34] in which researchers demonstrated a range of 3% to 18% artifact caused by metal scattering effects. The strong correlation between the tissue neogenesis in defects after eliminating the artifact-affected zone (Table 1) can be related to proportional bone apposition from the lateral and bottom walls of the host bone during peri-implant osseous wound repair (Fig 4). Meanwhile, the peri-implant structural parameters revealed some correlations with the interfacial biomechanics.[2,18] Taken together, it is reasonable to hypothesize that elimination of the scatter-affected peri-implant layer would provide a good prediction of dynamic functional changes during tissue-implant integration, and the present investigation successfully proved this hypothesis in both osteotomy defects in vivo (Fig 5).

In this study, the parameters from the specimens after implant removal to reduce the influence of metal scattering on the image were evaluated. Because the removal process may damage the interfacial tissues, in a previous study the authors had demonstrated no radiographically detectable tissue deformation of cylindric mini-implants via FE analysis.[20] Therefore, the correlation coefficient from the functionally relevant peri-implant layer tended to be lower in the OA defects (Fig 5), and evaluation from the osseous defect area demonstrated significantly lower correlation to the original area after eliminating the artifact-affected area at day 10, especially for BV and FCAM (Table 1). One explanation is that the new bone or woven bone near the interfacial area does not provide strong fixation. Although some initial contact osteogenesis occurred at the interface, the connection to any distant area of osteogenesis was still weak for establishing a favorable load distribution pattern to support the implant. However, the cellular activity adjacent to the bone surface cannot be observed from micro-CT imaging. Combined analysis with descriptive histology

is still recommended for the comprehensive evaluation of early wound healing events during osseointegration in preclinical investigations.

The inner peri-implant layer is believed to play a pivotal role because of higher stress accumulation in this area. FAM, optimized from simulated loading on the dental implant,[20] could be more clinically relevant than any individual structural parameter, and the value of FAM would not change significantly with an increase in the cumulative peri-implant layer. Thus, the correlation coefficient between FAM and interfacial stiffness reveals the efficiency of the functionally relevant peri-implant layers. Hedia demonstrated that the stress was concentrated at the interface and dropped significantly beyond a 150-μm zone under implant loading.[35] However, in the present study, the correlation between FCAM and IS was weaker within the first 200 μm in the OS group (Fig 5b). A possible explanation is that this 200-μm layer alone was incapable of bearing the implant load, and the isotropic elasticity of the element definition might not interpret the distribution of less-mature bone near the interface and the premature bone-implant contact. Therefore, the authors demonstrated a strong and consistent relationship between FAM and IS, which existed from the 300-μm peri-implant tissues in both OA and OS groups (Figs 5a and 5b). Removing the innermost 108 or 162 μm reduced the correlation (Fig 5) because it neglected the variations in the highest load–bearing interfacial tissues. Significant fluctuation of the correlation coefficient in the OS group was seen (Figs 5b and 5d), and this variation might relate to the highly heterogenous nature of the interfacial bone. Furthermore, while examining the micro-CT images with the implant present (Figs 5c and 5d), the trends in correlation coefficients also varied, whereas a strong correlation (r > 0.75) consistently existed only after the 162 μm peri-implant layer was removed. This discrepancy indicated that the metal scattering in the 108- to 162-μm layers from the micro-CT images still significantly influences analyses of the peri-implant structure. Consequently, the 300-μm-thick, functionally relevant peri-implant layer in all circumstances may be feasible to predict bone-implant contact stiffness and may be of clinical value in evaluating the progression of tissue-implant integration as well as for the prognosis of implant therapy. More detailed definition of element properties on the inner peri-implant layer may be indicated for future investigations on the early stage of tissue-implant integration.

CONCLUSION

Peri-implant interfacial structures, as seen in micro-computed tomographic imaging, and functional apparent moduli were dynamically correlated to the interfacial stiffness after correction of imaging artifacts in the preclinical model. The use of this concept may potentially enable noninvasive evaluation of the functional status during tissue-implant integration in clinical practice, although further definition of the elements near the tissue-implant interface may still be necessary. These data taken together offer strong support for the use of these approaches to biomechanical and imaging measures for determining osseointegration.

Acknowledgments

References

1. Franchi M, Fini M, Martini D, et al. Biological fixation of endosseous implants. Micron. 2005; 36:665–671. [PubMed: 16233979]

2. Turkyilmaz I, Sennerby L, McGlumphy EA, Tozum TF. Biomechanical aspects of primary implant stability: A human cadaver study. Clin Implant Dent Relat Res. 2009 Jun.11:113–119. [PubMed: 18422713]

3. Qian L, Todo M, Matsushita Y, Koyano K. Effects of implant diameter, insertion depth, and loading angle on stress/strain fields in implant/jawbone systems: Finite element analysis. Int J Oral Maxillofac Implants. 2009; 24:877–886. [PubMed: 19865628]

4. Soballe K, Hansen ES, B-Rasmussen H, Jorgensen PH, Bunger C. Tissue ingrowth into titanium and hydroxyapatite-coated implants during stable and unstable mechanical conditions. J Orthop Res. 1992; 10:285–299. [PubMed: 1311039]

5. Albrektsson T, Linder L. A method for short- and long-term in vivo study of the bone-implant interface. Clin Orthop Relat Res. 1981; (159):269–273. [PubMed: 7026120]

6. Marco F, Milena F, Gianluca G, Vittoria O. Peri-implant osteogenesis in health and osteoporosis. Micron. 2005; 36:630–644. [PubMed: 16182543]

7. Hedberg EL, Kroese-Deutman HC, Shih CK, et al. Methods: A comparative analysis of radiography, microcomputed tomography, and histology for bone tissue engineering. Tissue Eng. 2005; 11:1356–1367. [PubMed: 16259591]

8. Sykaras N, Woody RD, Iacopino AM, Triplett RG, Nunn ME. Osseointegration of dental implants complexed with rhBMP-2: A comparative histomorphometric and radiographic evaluation. Int J Oral Maxillofac Implants. 2004; 19:667–678. [PubMed: 15508982]

9. Brownfield LA, Weltman RL. Ridge preservation with or without an osteoinductive allograft. A clinical, radiographic, Micro-CT, and histologic study evaluating dimensional changes and new bone formation of the alveolar ridge. J Periodontol. 2012 May.83:581–589. [PubMed: 21942791]

10. Park CH, Abramson ZR, Taba M Jr, et al. Three-dimensional micro-computed tomographic imaging of alveolar bone in experimental bone loss or repair. J Periodontol. 2007; 78:273–281. [PubMed: 17274716]

11. Barrett JF, Keat N. Artifacts in CT: Recognition and avoidance. Radiographics. 2004; 24:1679–1691. [PubMed: 15537976]

12. Brånemark R, Ohrnell LO, Skalak R, Carlsson L, Brånemark PI. Biomechanical characterization of osseointegration: An experimental in vivo investigation in the beagle dog. J Orthop Res. 1998; 16:61–69. [PubMed: 9565075]

13. Atsumi M, Park SH, Wang HL. Methods used to assess implant stability: Current status. Int J Oral Maxillofac Implants. 2007; 22:743–754. [PubMed: 17974108]

14. Johansson CB, Gretzer C, Jimbo R, Mattisson I, Ahlberg E. Enhanced implant integration with hierarchically structured implants: A pilot study in rabbits. Clin Oral Implants Res. 2012 Aug. 23:943–953. [PubMed: 21722190]

15. Johansson CB, Han CH, Wennerberg A, Albrektsson T. A quantitative comparison of machined commercially pure titanium and titanium-aluminum- vanadium implants in rabbit bone. Int J Oral Maxillofac Implants. 1998; 13:315–321. [PubMed: 9638001]

16. Tozum TF, Turkyilmaz I, McGlumphy EA. Relationship between dental implant stability determined by resonance frequency analysis measurements and peri-implant vertical defects: An in vitro study. J Oral Rehabil. 2008; 35:739–744. [PubMed: 18422511]

17. Motoyoshi M, Yoshida T, Ono A, Shimizu N. Effect of cortical bone thickness and implant placement torque on stability of orthodontic mini-implants. Int J Oral Maxillofac Implants. 2007; 22:779–784. [PubMed: 17974113]

18. Ramp LC, Jeffcoat RL. Dynamic behavior of implants as a measure of osseointegration. Int J Oral Maxillofac Implants. 2001; 16:637–645. [PubMed: 11669245]

19. Berzins A, Shah B, Weinans H, Sumner DR. Nondestructive measurements of implant-bone interface shear modulus and effects of implant geometry in pull-out tests. J Biomed Mater Res. 1997; 34:337–340. [PubMed: 9086403]

20. Chang PC, Seol YJ, Kikuchi N, Goldstein SA, Giannobile WV. Functional apparent moduli as predictors of oral implant osseointegration dynamics. J Biomed Mater Res B Appl Biomater. 2010; 94:118–126. [PubMed: 20524185]

21. Risselada M, van Bree H, Kramer M, et al. Evaluation of nonunion fractures in dogs by use of B-mode ultrasonography, power Doppler ultrasonography, radiography, and histologic examination. Am J Vet Res. 2006; 67:1354–1361. [PubMed: 16881847]

22. Chang PC, Seol YJ, Cirelli JA, et al. PDGF-B gene therapy accelerates bone engineering and oral implant osseointegration. Gene Ther. 2010; 17:95–104. [PubMed: 19741730]

23. Keller TS. Predicting the compressive mechanical behavior of bone. J Biomech. 1994; 27:1159–1168. [PubMed: 7929465]

24. Kelly DJ, Prendergast PJ. Prediction of the optimal mechanical properties for a scaffold used in osteochondral defect repair. Tissue Eng. 2006; 12:2509–2519. [PubMed: 16995784]

25. Koca OL, Eskitascioglu G, Usumez A. Three-dimensional finite-element analysis of functional stresses in different bone locations produced by implants placed in the maxillary posterior region of the sinus floor. J Prosthet Dent. 2005; 93:38–44. [PubMed: 15623996]

26. Palmquist A, Emanuelsson L, Brånemark R, Thomsen P. Biomechanical, histological and ultrastructural analyses of laser micro- and nano-structured titanium implant after 6 months in rabbit. J Biomed Mater Res B Appl Biomater. 2011; 97:289–298. [PubMed: 21394900]

27. Turkyilmaz I, McGlumphy EA. Is there a lower threshold value of bone density for early loading protocols of dental implants? J Oral Rehabil. 2008; 35:775–781. [PubMed: 18482347]

28. Ersoy AE, Turkyilmaz I, Ozan O, McGlumphy EA. Reliability of implant placement with stereolithographic surgical guides generated from computed tomography: Clinical data from 94 implants. J Periodontol. 2008; 79:1339–1345. [PubMed: 18672982]

29. Terzioglu H, Akkaya M, Ozan O. The use of a computerized tomography- based software program with a flapless surgical technique in implant dentistry: A case report. Int J Oral Maxillofac Implants. 2009; 24:137–142. [PubMed: 19344037]

30. Van Oossterwyck H, Duyck J, Vander Sloten J, et al. Use of microfocus computerized tomography as a new technique for characterizing bone tissue around oral implants. J Oral Implantol. 2000; 26:5–12. [PubMed: 11831302]

31. Stoppie N, van der Waerden JP, Jansen JA, Duyck J, Wevers M, Naert IE. Validation of microfocus computed tomography in the evaluation of bone implant specimens. Clin Implant Dent Relat Res. 2005; 7:87–94. [PubMed: 15996355]

32. Rebaudi A, Koller B, Laib A, Trisi P. Microcomputed tomographic analysis of the peri-implant bone. Int J Periodontics Restorative Dent. 2004; 24:316–325. [PubMed: 15446401]

33. Butz F, Ogawa T, Chang TL, Nishimura I. Three-dimensional bone-implant integration profiling using micro-computed tomography. Int J Oral Maxillofac Implants. 2006; 21:687–695. [PubMed: 17066629]

34. Jakel O, Reiss P. The influence of metal artefacts on the range of ion beams. Phys Med Biol. 2007; 52:635–644. [PubMed: 17228110]

35. Hedia HS. Effect of coating thickness and its material on the stress distribution for dental implants. J Med Eng Technol. 2007; 31:280–287. [PubMed: 17566931]
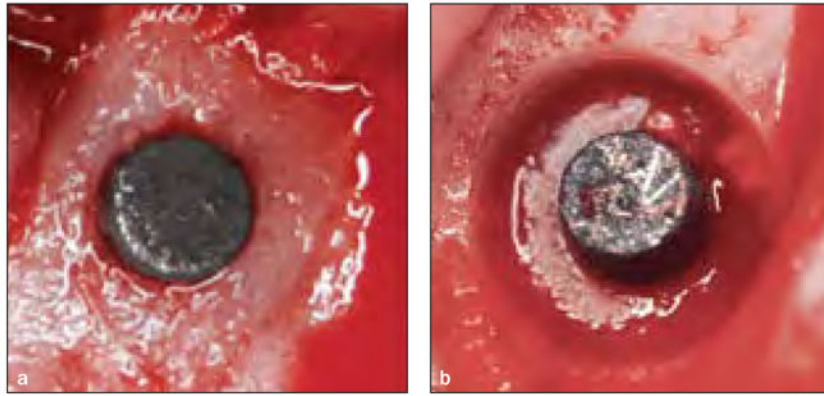
Fig 1.
Animal surgery. *(a)* 1-mm-diameter titanium implant in a rat maxilla in the osteotomy-alone (OA) group. *(b)* In the osteotomy– osseous defect (OS) group, a 0.6×1-mm circumferential osseous implant was created around the implant.
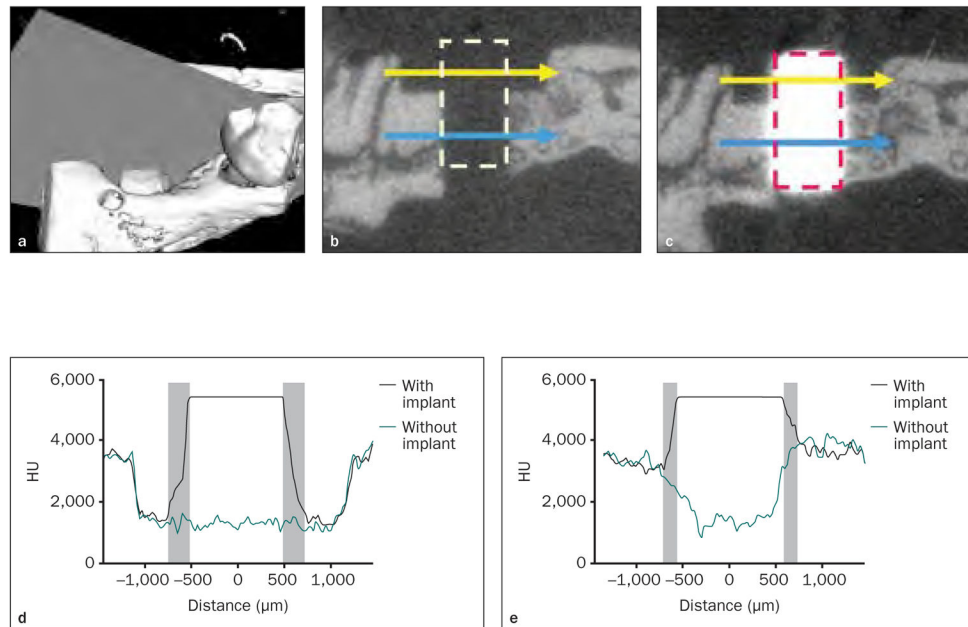
Fig 2. Effects of metal scattering on micro-CT imaging

Fig 2a Three-dimensional micro-CT image. A single slice was selected from the central sagittal plane crossing in the osseous defect (*grey plane*).

Figs 2b and 2c Two-dimensional slices of micro-CT imaging (*left*) before and (*right*) after implant placement. The area marked by the dashed line refers to the space occupied by the titanium implant; the yellow line indicates the OS defect region; the blue line indicates the OA region.

Figs 2d and 2e Distribution of HU values before and after implant placement. (*d*) In the OS area, a 126-μm blurred zone (*gray zones*) on the left and a 162-μm zone on the right side of the implant were noted. (*e*) In the OA area, a 108-μm radiographic artifact (*gray zones*) was noted on both sides of the implant.
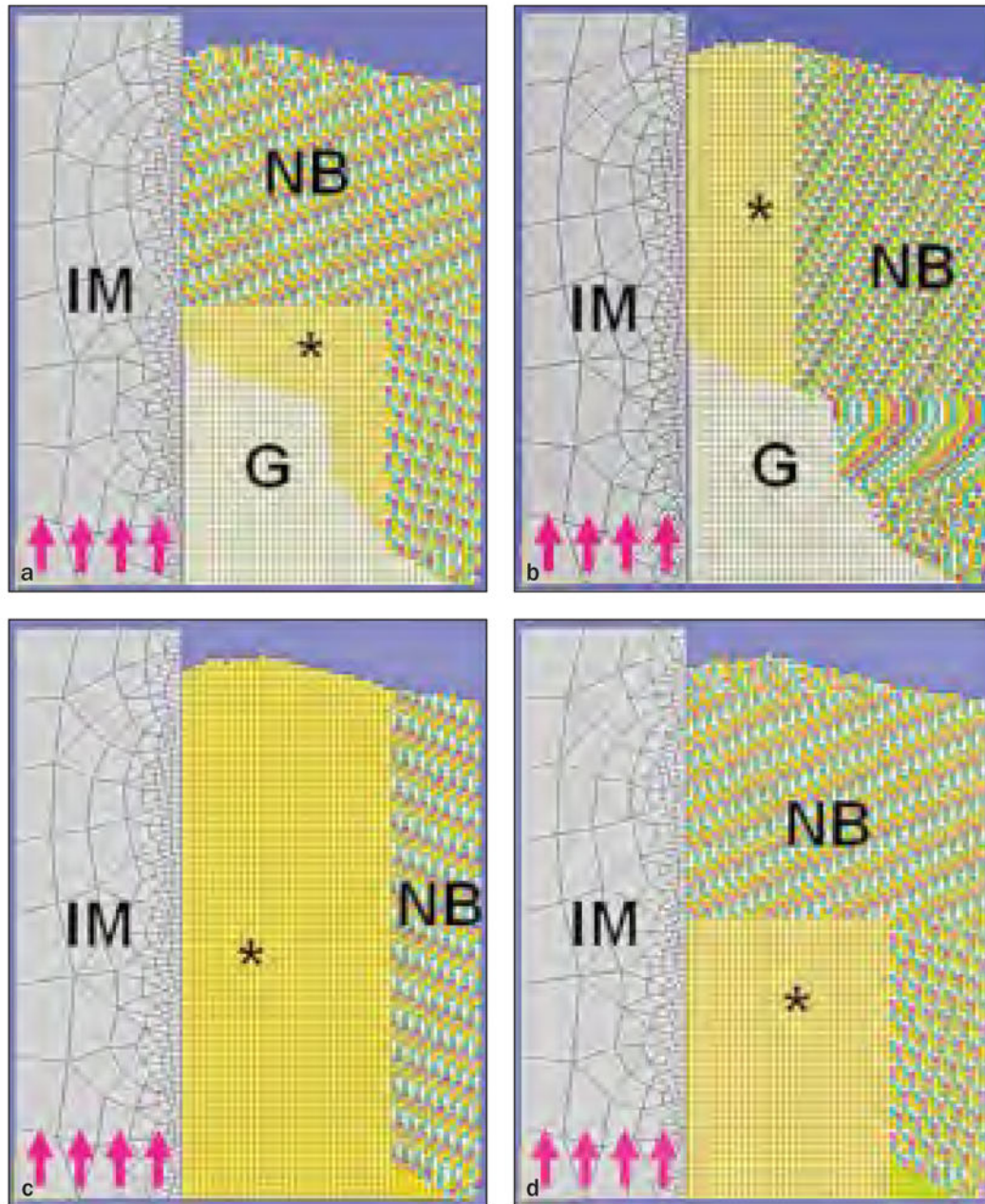
Fig 3.

Figs 3a to 3d The FE model for calculating FBAM and FCAM. IM = titanium implant; G = granulation tissue; NB = native bone; MS = maxillary sinus; asterisks refer to area of investigation; purple arrows indicate the direction of simulated load.
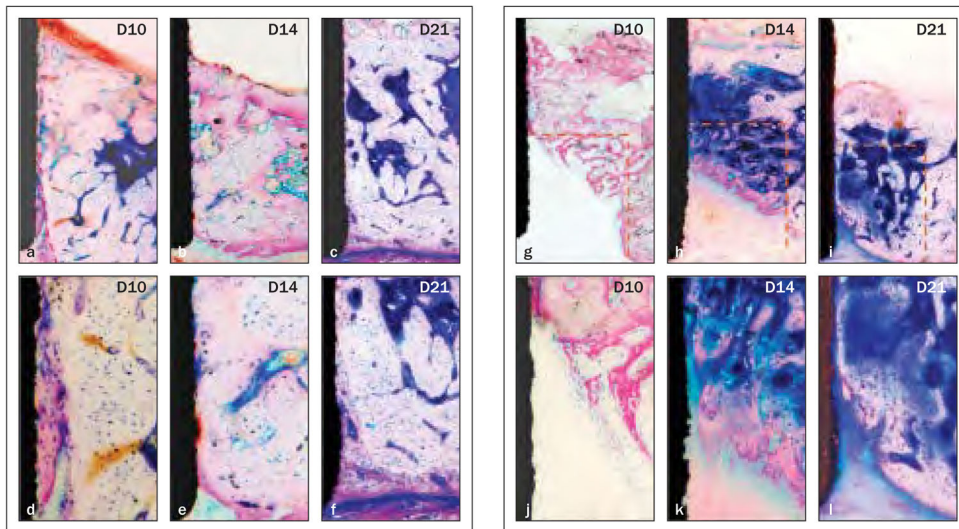
Fig 3a FBAM for osseous wound repair.

Fig 3b FBAM for interfacial osseointegration.

Fig 3c FCAM for interfacial osseointegration.

**Fig 3d** FCAM for osseous wound repair.

Fig 4. Bone apposition from the base and lateral walls of osteotomy over time (methylene blue and acid fuchsin; original magnification ×40 in the top row, ×200 in the bottom row)
Figs 4a to 4f Defects in the OA group. At day 10 (*left-hand column*), a 0- to 50-μm gap (dashed line in the first column) on the interface was filled by new bone. Significant maturation of the interfacial tissue was evident (*middle column*) on day 14 and (*right-hand column*) on day 21.
Figs 4g to 4i Defects in the OS group. (*Left-hand column*) A woven trabecular bone structure grew from the border of the defect at day 10. Significant bone maturation and apposition were noted (*middle column*) on day 14 and (*right-hand column*) day 21.
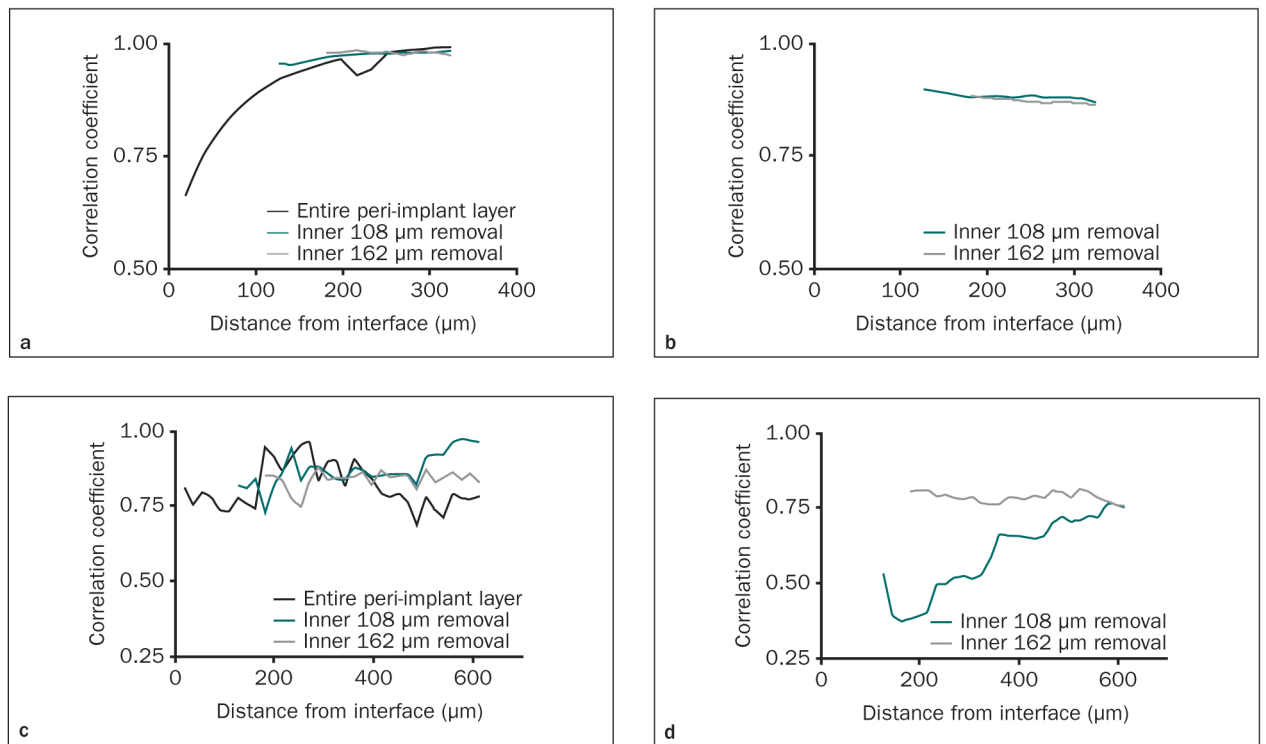
Fig 5.

Figs 5a to 5d Correlation between functional apparent moduli and interfacial stiffness after eliminating the "artifact layers." The correlation coefficient between FBAM and IS was examined in the OA group with increasing peri-implant thickness (*a*) after implant removal and (*b*) with the implant present, and correlation between peri-implant functional composite tissue apparent modulus (FCAM) and IS was examined in osteotomy plus osseous defect (OS) group with the increasing peri-implant thickness (*c*) after implant removal and (*d*) with the implant present. Either the 108-μm or the 162-μm innermost layer was assumed as the "artifact layer" and eliminated for the analyses (ie, analyses started at 126 and 180 μm from the interface, respectively).

Table 1

Correlation of Structural Parameters and FAM Between Artifact and Nonartifact Situations in Implant Osteotomy Defect Zones

	Mean (standard deviation)			Correlation to 0 μm (r)	
	0 μm	108 μm	162 μm	108 μm	162 μm
BV (mm³)					
Overall (n = 12)	0.137 (0.012)	0.118 (0.012)[†]	0.111 (0.012)[†]	0.955	0.934
Day 10 (n = 6)	0.135 (0.006)[*]	0.117 (0.005)[*†]	0.110 (0.005)[*†]	0.615	0.442
Day 14 (n = 6)	0.138 (0.016)	0.119 (0.017)[†]	0.111 (0.017)[†]	0.994	0.995
BMC (10⁶ HU)					
Overall (n = 12)	3.95 (0.83)	3.41 (0.67)[†]	3.21 (0.62)[†]	0.989	0.980
Day 10 (n = 6)	3.40 (0.74)[*]	2.94 (0.57)[*†]	2.77 (0.51)[*†]	0.984	0.970
Day 14 (n = 6)	4.50 (0.49)	3.87 (0.38)[†]	3.64 (0.35)[†]	0.971	0.949
FBAM (MPa)					
Overall (n = 12)	7,943 (1,281)	8,153 (1,385)	8,334 (1,424)	0.987	0.956
Day 10 (n = 6)	7,668 (742)	7,868 (976)	8,090 (1,162)	0.964	0.900
Day 14 (n = 6)	8,201 (1,750)	8,431 (1,831)	8,562 (1,783)	0.996	0.989
FCAM (MPa)					
Overall (n = 12)	6,028 (2,981)	6,632 (3,004)	6,785 (2,824)	0.982	0.933
Day 10 (n = 6)	4,194 (710)	4,727 (1,079)	5,143 (1,422)	0.787	0.414
Day 14 (n = 6)	7,871 (3,350)	8,519 (3,202)	8,428 (3,052)	0.989	0.961

[*] Significant difference versus day 14 ($P < .05$);

[†] Significant difference to removal of 0-μm layer situation ($P < .05$).